A Novel Thick Ellipsoid Approach for Verified Outer and Inner State Enclosures of Discrete-Time Dynamic Systems

Andreas Rauh * **Luc Jaulin** *

* *Lab-STICC, ENSTA Bretagne, 29806 Brest, France (e-mail: Andreas.Rauh@interval-methods.de, lucjaulin@gmail.com)*

Abstract: Simulating dynamic systems with bounded uncertainty in initial conditions and selected parameters is a common task for the reliability analysis of closed-loop control structures as well as for a simulation-based parameter identification on the basis of uncertain measurements. However, dealing with bounded uncertainty is not a trivial task. On the one hand, the naive application of interval analysis often leads to excessively large bounds which may yield state enclosures that are by far too pessimistic to be useful in practice. On the other hand, the use of grid-based or probabilistic and Monte-Carlo like simulation approaches suffers from the disadvantage that they do not provide a guarantee of the correctness of the obtained solutions. Using insufficiently many or badly chosen samples may lead to the phenomenon that critical system states are not detected so that the computed results underestimate the range of reachable states. Therefore, a novel ellipsoidal state enclosure technique is presented which does not require the online solution of linear matrix inequalities (LMIs). It uses the newly introduced representation of state domains by means of thick ellipsoids. These domains simultaneously represent inner and outer enclosures of the reachable states and directly provide a measure for the tightness of the obtained results, regardless of whether the system is linear or nonlinear or whether it is stable or not.

Keywords: Robustness analysis, Bounded Uncertainty, Ellipsoidal state enclosures, Thick ellipsoids, Verified simulation, Interval analysis.

1. INTRODUCTION

The use of interval analysis for a reliable parameter identification has been studied for numerous applications such as high-temperature fuel cells or other thermal systems (Rauh and Kersten, 2020). Although it has been possible for these applications to derive point-valued bounding systems due to the property of cooperativity (i.e., the monotonicity of the trajectories with respect to initial conditions and selected parameters, see Rauh and Kersten (2020)), many models in engineering as well as computational physics or biology do not posses this property. Then, it is either necessary to find similarity transformations into a new frame of coordinates in which these monotonicity properties are satisfied or to use more general set-valued simulation approaches that directly work on the complete bounded parameter domains of interest, see Mazenc and Bernard (2010); Rauh et al. (2019). The second approach is necessary especially in cases where transformations into a cooperative form are either not available or prohibitively conservative due to an unavoidable wrapping effect if the system representation may either have real or complex eigenvalues depending on the actual parameter value.

In this paper, we restrict ourselves to the set-valued simulation of discrete-time systems. For those, a naive use of interval analysis (Jaulin et al., 2001; Moore et al., 2009) may lead to a blowup of the widths of state enclosures even if the dynamics are linear. The reason for such behavior is the solution representation by axis-aligned boxes which are propagated further in subsequent time steps. Despite its simplicity, this box representation has the drawback that information about the correlation between individual components of the state vector is lost by the axis-aligned representation and that — due to this so-called wrapping effect — a model is actually evaluated that is more conservative than necessary. A possible countermeasure, at least for (quasi-)linear systems, is an iterated evaluation that tries to relate the actual system states in a recursive manner to the initial conditions. As shown in Rauh et al. (2007), the corresponding procedures rely on storing modified interval-valued system matrices in addition to the actual state enclosures. Alternatively, specific implementations of affine system and uncertainty representations could be used (Stolfi et al., 2003).

In general, the use of axis-aligned boxes has the disadvantage that each transformation (even the application of a pure rotation matrix) leads to pessimism. In contrast, the use of ellipsoids (Kurzhanskii and Vályi, 1997; Kurzhanskiy and Varaiya, 2006; Neumaier, 1993) is often more efficient, when in a suitably chosen coordinate frame linear transformations such as rotation and scaling can be carried out in an overestimation-free manner. Moreover, ellipsoids are natural representations of state domains if quadratic Lyapunov function approaches are used for the analysis of stability properties. Therefore, we introduce a novel uncertainty model — called *thick ellipsoids* — in this paper. It allows us, in contrast to the works of

Neumaier (1993) as well as Kurzhanskii and Vályi (1997), to simultaneously represent inner and outer enclosures of reachable state domains and in such a way provides a direct measure for the worst-case overestimation that is included in the result of a dynamic system simulation. Thick ellipsoids can be interpreted as a generalization of a similar concept that was already introduced in terms of *thick intervals* and *thick boxes*, where each of the interval endpoints or interval edges is represented itself by an interval-valued quantity (Desrochers and Jaulin, 2017). In contrast to existing ellipsoidal approaches for state estimation, the proposed technique avoids the online solution of LMIs or complex minmax optimization tasks (Dabbene and Henrion, 2013; Durieu et al., 1996) and significantly reduces computational complexity, cf. Rauh et al. (2021).

This paper is structured as follows. In Sec. 2, the new notion of thick ellipsoids is introduced. Based on this definition, a recursive simulation algorithm for discrete-time dynamic system models is derived in Sec. 3. This simulation algorithm relies on a Cholesky factorization-based representation of ellipsoids in a multi-dimensional state space. Sec. 4 provides simulation results for three different benchmark applications, before conclusions and an outlook on future work are given in Sec. 5.

Notation: Throughout this paper, $\|\cdot\|$ represents (an interval extension of) the Euclidean norm of the corresponding vector-valued argument (Rauh and Jaulin, 2021).

2. THICK ELLIPSOIDS

Definition 1. (Thick ellipsoid). Define a thick ellipsoid $(\!(\mathcal{E})\!) = (\!(\mathcal{E})\!)\left(\boldsymbol{\mu}, \boldsymbol{\Gamma}, \left[\underline{\rho}\ ;\ \overline{\rho}\right]\right)$ as a subset of the power set $\mathcal{P}(\mathbb{R}^n)$ so that

$$(\!(\mathcal{E})\!) = \left\{\mathcal{A} \in \mathcal{P}(\mathbb{R}^n) \mid \mathcal{E}^{\mathrm{I}} \subseteq \mathcal{A} \subseteq \mathcal{E}^{\mathrm{O}}\right\} \tag{1}$$

with

$$\mathcal{E}^{\mathrm{I}} = \left\{\mathbf{x} \in \mathbb{R}^n \mid (\mathbf{x}-\boldsymbol{\mu})^T \left(\underline{\rho}\boldsymbol{\Gamma}\right)^{-T} \left(\underline{\rho}\boldsymbol{\Gamma}\right)^{-1} (\mathbf{x}-\boldsymbol{\mu}) \leq 1\right\},$$
$$\mathcal{E}^{\mathrm{O}} = \left\{\mathbf{x} \in \mathbb{R}^n \mid (\mathbf{x}-\boldsymbol{\mu})^T (\overline{\rho}\boldsymbol{\Gamma})^{-T} (\overline{\rho}\boldsymbol{\Gamma})^{-1} (\mathbf{x}-\boldsymbol{\mu}) \leq 1\right\} \tag{2}$$

and $0 \leq \underline{\rho} \leq \overline{\rho}$.

An illustration of this thick ellipsoid is given in Fig. 1.

Definition 2. (Thick ellipsoid binary operators and function extensions). A thick ellipsoid extension of the binary operators [1] $\diamond \in \{+, -, \cdot, /, \cup, \cap\}$ satisfies the relation

$$\begin{cases} \mathcal{A} \in (\!(\mathcal{A})\!)\ , \quad \mathcal{B} \in (\!(\mathcal{B})\!) \\ \mathcal{C} = \mathcal{A} \diamond \mathcal{B} \end{cases} \implies \mathcal{C} \in (\!(\mathcal{A})\!) \diamond (\!(\mathcal{B})\!)\ . \tag{3}$$

The quantity $(\!(\mathcal{C})\!) = (\!(\mathcal{A})\!) \diamond (\!(\mathcal{B})\!)$ is also a thick ellipsoid, which is typically neither minimal with respect to its width nor uniquely defined. Analogously, $(\!(\mathbf{f})\!)$ is a thick ellipsoid function extension of $\mathbf{f} : \mathbb{R}^n \mapsto \mathbb{R}^m$, if

$$\begin{cases} \mathcal{A} \in (\!(\mathcal{A})\!) \\ \mathcal{B} = \mathbf{f}(\mathcal{A}) \end{cases} \implies \mathcal{B} \in (\!(\mathcal{B})\!) = (\!(\mathbf{f})\!)(\!(\mathcal{A})\!)\ . \tag{4}$$

3. RECURSIVE SIMULATION ALGORITHM

3.1 Theoretical Background

Consider a finite-dimensional discrete-time system model

$$\mathbf{x}_{k+1} = \mathbf{f}(\mathbf{x}_k)\ ,\quad \mathbf{f} : \mathbb{R}^n \mapsto \mathbb{R}^n\ , \tag{5}$$

[1] As in classical interval arithmetic (Jaulin et al., 2001), the value zero must not belong to the denominator expression.

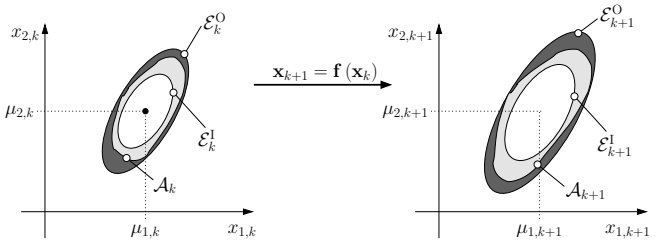

Fig. 1. Definition of a thick ellipsoid $(\!(\mathcal{E})\!)_k$ enclosing the domain $\mathcal{A}_k$ and its mapping via the system model (5).

where $\mathbf{f}$ is assumed to be differentiable. Given a thick ellipsoid representation $(\!(\mathcal{E})\!)_k = (\!(\mathcal{E})\!)\left(\boldsymbol{\mu}_k, \boldsymbol{\Gamma}_k, \left[\underline{\rho}_k\ ;\ \overline{\rho}_k\right]\right)$ at the time instant k, it is desired to determine a thick ellipsoid $(\!(\mathcal{E})\!)_{k+1} = (\!(\mathcal{E})\!)\left(\boldsymbol{\mu}_{k+1}, \boldsymbol{\Gamma}_{k+1}, \left[\underline{\rho}_{k+1}\ ;\ \overline{\rho}_{k+1}\right]\right)$ at the instant $k+1$ that is defined such that $\mathcal{E}_{k+1}^{\mathrm{I}}$ is an inner boundary containing certainly reachable states and $\mathcal{E}_{k+1}^{\mathrm{O}}$ is a guaranteed outer enclosure, see Fig. 1.

Theorem 3. (Thick ellipsoid enclosures). Define the state enclosure at the time instant k by the thick ellipsoid $(\!(\mathcal{E})\!)_k$ according to Def. 1. For a differentiable state equation (5), with

$$\mathbf{A}_k = \frac{\partial \mathbf{f}}{\partial \mathbf{x}_k}(\boldsymbol{\mu}_k) \quad \text{invertible}\ , \tag{6}$$

$$(\!(\mathcal{E})\!)_{k+1} = (\!(\mathcal{E})\!)\left(\boldsymbol{\mu}_{k+1}, \boldsymbol{\Gamma}_{k+1}, \underline{\rho}_{k+1}, \overline{\rho}_{k+1}\right) \tag{7}$$

is a thick ellipsoid enclosure of the solution set $\mathbf{f}\left((\!(\mathcal{E})\!)_k\right)$ with

$$\boldsymbol{\mu}_{k+1} = \mathbf{f}(\boldsymbol{\mu}_k) \quad \text{and} \quad \boldsymbol{\Gamma}_{k+1} = \mathbf{A}_k \cdot \boldsymbol{\Gamma}_k \tag{8}$$

as well as

$$\underline{\rho}_{k+1} = (1 - \rho_{\mathrm{I},k}) \cdot \underline{\rho}_k \quad \text{and} \quad \overline{\rho}_{k+1} = (1 + \rho_{\mathrm{O},k}) \cdot \overline{\rho}_k\ . \tag{9}$$

Here,

$$\rho_{\mathrm{I},k} = \max_{\|\tilde{\mathbf{x}}_k\| \leq 1} \left\| \tilde{\mathbf{b}}_{\mathrm{I},k}(\tilde{\mathbf{x}}_k) \right\|\ , \tag{10}$$

$$\tilde{\mathbf{b}}_{\mathrm{I},k}(\tilde{\mathbf{x}}_k) = \underline{\rho}_k^{-1} \boldsymbol{\Gamma}_k^{-1} \mathbf{A}_k^{-1} \cdot \left(\mathbf{f}\left(\underline{\rho}_k \boldsymbol{\Gamma}_k \tilde{\mathbf{x}}_k + \boldsymbol{\mu}_k\right) - \mathbf{f}(\boldsymbol{\mu}_k)\right) - \tilde{\mathbf{x}}_k \tag{11}$$

and

$$\rho_{\mathrm{O},k} = \max_{\|\tilde{\mathbf{x}}_k\| \leq 1} \left\| \tilde{\mathbf{b}}_{\mathrm{O},k}(\tilde{\mathbf{x}}_k) \right\|\ , \tag{12}$$

$$\tilde{\mathbf{b}}_{\mathrm{O},k}(\tilde{\mathbf{x}}_k) = \overline{\rho}_k^{-1} \boldsymbol{\Gamma}_k^{-1} \mathbf{A}_k^{-1} \cdot \left(\mathbf{f}\left(\overline{\rho}_k \boldsymbol{\Gamma}_k \tilde{\mathbf{x}}_k + \boldsymbol{\mu}_k\right) - \mathbf{f}(\boldsymbol{\mu}_k)\right) - \tilde{\mathbf{x}}_k\ . \tag{13}$$

Proof. The proof consists of two parts. First, the outer boundary $\mathcal{E}_{k+1}^{\mathrm{O}}$ of the thick ellipsoid $(\!(\mathcal{E})\!)_{k+1}$ is verified. For that purpose, set

$$\tilde{\mathbf{x}}_k = \overline{\rho}_k^{-1} \cdot \boldsymbol{\Gamma}_k^{-1} \cdot (\mathbf{x}_k - \boldsymbol{\mu}_k)\ . \tag{14}$$

According to Def. 1, $\mathcal{E}_k^{\mathrm{O}}$ as the outer bound of $(\!(\mathcal{E})\!)_k$ becomes

$$\tilde{\mathbf{x}}_k \in \mathcal{S}_x := \left\{\tilde{\mathbf{x}}_k \mid \|\tilde{\mathbf{x}}_k\| \leq 1\right\}\ . \tag{15}$$

Second, define

$$\tilde{\mathbf{x}}_{k+1} = \tilde{\mathbf{x}}_k + \tilde{\mathbf{b}}_{\mathrm{O},k}(\tilde{\mathbf{x}}_k) \tag{16}$$

with $\tilde{\mathbf{b}}_{\mathrm{O},k}(\tilde{\mathbf{x}}_k)$ given in (13). Hence, according to the triangle inequality,

$$\|\tilde{\mathbf{x}}_{k+1}\| \leq \|\tilde{\mathbf{x}}_k\| + \left\|\tilde{\mathbf{b}}_{\mathrm{O},k}(\tilde{\mathbf{x}}_k)\right\| = 1 + \rho_{\mathrm{O},k} \tag{17}$$

holds with

$$\rho_{\mathrm{O},k} = \arg\min_{\rho \in \mathbb{R}^+} \left\{\rho \in \mathbb{R}^+ \mid \left\|\tilde{\mathbf{b}}_{\mathrm{O},k}(\tilde{\mathbf{x}}_k)\right\| \leq \rho\ ,\ \ \forall \tilde{\mathbf{x}}_k \in \mathcal{S}_x\right\}. \tag{18}$$

Alternatively, (16) can be expressed as $\tilde{\mathbf{x}}_{k+1} \in \mathcal{S}_x \oplus \mathcal{S}^{\mathrm{O}}_{b,k}$, where $\oplus$ is the Minkowski sum of two sets and

$$\tilde{\mathbf{b}}_{\mathrm{O},k}\left(\tilde{\mathbf{x}}_k\right) \in \mathcal{S}^{\mathrm{O}}_{b,k} := \left\{\tilde{\mathbf{x}}_k \mid \|\tilde{\mathbf{x}}_k\| \leq \rho_{\mathrm{O},k}\right\} \ . \tag{19}$$

Therefore, $\tilde{\mathbf{x}}_{k+1}$ belongs to a ball of radius $1+\rho_{\mathrm{O},k}$ as illustrated in Fig. 2. According to (13) and (16), the equality

$$\tilde{\mathbf{x}}_{k+1} = \overline{\rho}_k^{-1} \cdot \boldsymbol{\Gamma}_k^{-1} \cdot \mathbf{A}_k^{-1} \cdot \left(\mathbf{x}_{k+1} - \boldsymbol{\mu}_{k+1}\right) \tag{20}$$

holds. Substituting this equality into (17) yields the outer boundary $\mathcal{E}^{\mathrm{O}}_{k+1}$ of the thick ellipsoid according to (7)–(8).

For the second part of the proof, set

$$\tilde{\mathbf{x}}_k = \underline{\rho}_k^{-1} \cdot \boldsymbol{\Gamma}_k^{-1} \cdot \left(\mathbf{x}_k - \boldsymbol{\mu}_k\right) \tag{21}$$

instead of (14). Then,

$$\tilde{\mathbf{x}}_{k+1} = \tilde{\mathbf{x}}_k + \tilde{\mathbf{b}}_{\mathrm{I},k}\left(\tilde{\mathbf{x}}_k\right) \tag{22}$$

with $\tilde{\mathbf{b}}_{\mathrm{I},k}\left(\tilde{\mathbf{x}}_k\right)$ given in (11) yields

$$\tilde{\mathbf{b}}_{\mathrm{I},k}\left(\tilde{\mathbf{x}}_k\right) \in \mathcal{S}^{\mathrm{I}}_{b,k} := \left\{\tilde{\mathbf{x}}_k \mid \|\tilde{\mathbf{x}}_k\| \leq \rho_{\mathrm{I},k}\right\} \tag{23}$$

with

$$\rho_{\mathrm{I},k} = \underset{\rho \in \mathbb{R}^+}{\arg\min} \left\{\rho \in \mathbb{R}^+ \mid \left\|\tilde{\mathbf{b}}_{\mathrm{I},k}\left(\tilde{\mathbf{x}}_k\right)\right\| \leq \rho \ , \quad \forall \tilde{\mathbf{x}}_k \in \mathcal{S}_x\right\} . \tag{24}$$

The maximum ellipsoid in the interior of the solution set that is *parallel* to the outer domain boundary $\mathcal{E}^{\mathrm{O}}_{k+1}$ results from the Minkowski difference $\mathcal{S}^{\mathrm{I}} = \mathcal{S}_x \ominus \mathcal{S}^{\mathrm{I}}_{b,k}$. Applying Eq. (20) after the replacement of $\overline{\rho}_k$ by $\underline{\rho}_k$ leads to $\mathcal{E}^{\mathrm{I}}_{k+1}$ as an inner approximation of $\mathcal{S}^{\mathrm{I}}$. Summarizing both $\mathcal{E}^{\mathrm{I}}_{k+1}$ and $\mathcal{E}^{\mathrm{O}}_{k+1}$ into the single thick ellipsoid $\langle\!\langle\mathcal{E}\rangle\!\rangle_{k+1}$, cf. (7), completes the proof. □

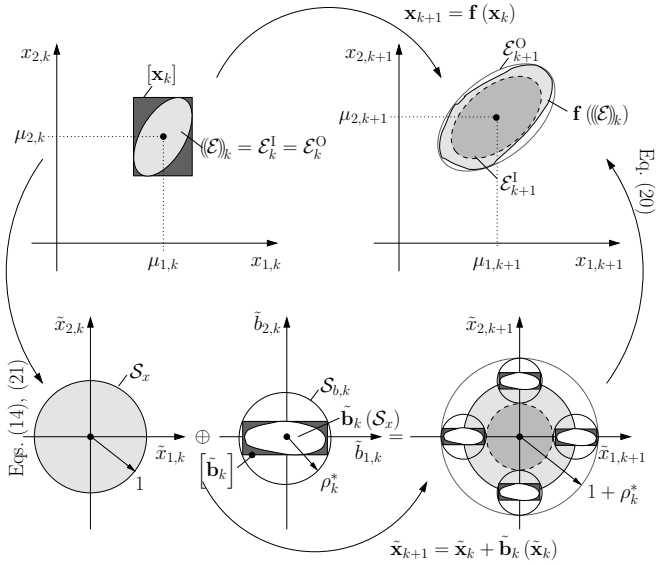

Fig. 2. Recursive computation of ellipsoidal state enclosures (simplified for $\langle\!\langle\mathcal{E}\rangle\!\rangle_k = \mathcal{E}^{\mathrm{I}}_k = \mathcal{E}^{\mathrm{O}}_k$, leading to $\mathcal{S}_{b,k} = \mathcal{S}^{\mathrm{O}}_{b,k} = \mathcal{S}^{\mathrm{I}}_{b,k}$, $\tilde{\mathbf{b}}_k = \tilde{\mathbf{b}}_{\mathrm{O},k} = \tilde{\mathbf{b}}_{\mathrm{I},k}$ and $\rho^*_k = \rho_{\mathrm{O},k} = \rho_{\mathrm{I},k}$ in the illustration).

Remark 4. Due to the fact that the matrices $\boldsymbol{\Gamma}_k$ are typically not symmetric in the recursive evaluation of the ellipsoidal simulation procedure, the following algorithm is based on a Cholesky-like decomposition of the shape matrix $\boldsymbol{\Gamma}_k \boldsymbol{\Gamma}_k^T$ of an ellipsoid. The factorized representation of the shape matrix simplifies the implementation of a recursive simulation procedure, see line 3 in Algorithm 1.

Remark 5. Eqs. (11) and (13) require that the Jacobian $\mathbf{A}_k$ at the midpoint of the thick ellipsoid $\langle\!\langle\mathcal{E}\rangle\!\rangle_k$ is invertible. If this is not the case, the shape matrix can be approximated in practice by using a representative slope within the domain of interest or with the help of the matrix square root of the covariance matrix $\mathrm{cov}\left(\mathbf{f}\left(\mathcal{X}_k\right)\right)$, where

$$\mathcal{X}_k = \left[\boldsymbol{\mu}_k - \boldsymbol{\Delta}_{1,k} \ \ldots \ \boldsymbol{\mu}_k - \boldsymbol{\Delta}_{n,k} \ \boldsymbol{\mu}_k + \boldsymbol{\Delta}_{1,k} \ \ldots \ \boldsymbol{\mu}_k + \boldsymbol{\Delta}_{n,k}\right] \tag{25}$$

with $\boldsymbol{\Delta}_{i,k}$, $i \in \{1,\ldots,n\}$, are determined in analogy to the sigma points of an Unscented Kalman Filter according to

$$\boldsymbol{\Delta}_{i,k} = \sqrt{n} \cdot \boldsymbol{\Gamma}_{i,k} \quad \text{with} \quad \boldsymbol{\Gamma}_k = \left[\boldsymbol{\Gamma}_{1,k} \ \ldots \ \boldsymbol{\Gamma}_{n,k}\right] \ . \tag{26}$$

3.2 Implementation of the Algorithm

The implementation of the thick ellipsoid simulation procedure is summarized in Algorithm 1.

Algorithm 1: Recursive simulation approach

input : $\mathbf{f}\left(\mathbf{x}_k\right)$, $\{\boldsymbol{\mu}_k, \boldsymbol{\Gamma}_k, \underline{\rho}_k, \overline{\rho}_k\}$
output: $\{\boldsymbol{\mu}_{k+1}, \boldsymbol{\Gamma}_{k+1}, \underline{\rho}_{k+1}, \overline{\rho}_{k+1}\}$

1 $\quad \boldsymbol{\mu}_{k+1} = \mathbf{f}\left(\boldsymbol{\mu}_k\right)$
2 $\quad \mathbf{A}_k = \frac{\partial \mathbf{f}}{\partial \mathbf{x}_k}\left(\boldsymbol{\mu}_k\right)$
3 $\quad \boldsymbol{\Gamma}_{k+1} = \mathbf{A}_k \cdot \boldsymbol{\Gamma}_k$
4 $\quad \rho_{\mathrm{I},k} \leftarrow$ **Compute norm** depending on $\underline{\rho}_k$
5 $\quad \rho_{\mathrm{O},k} \leftarrow$ **Compute norm** depending on $\overline{\rho}_k$
6 $\quad \underline{\rho}_{k+1} = (1 - \rho_{\mathrm{I},k}) \cdot \underline{\rho}_k$
7 $\quad \overline{\rho}_{k+1} = (1 + \rho_{\mathrm{O},k}) \cdot \overline{\rho}_k$

Algorithm 2: Compute norm

input : $\boldsymbol{\mu}_k, \boldsymbol{\Gamma}_k, \boldsymbol{\Gamma}_{k+1}, \rho_\iota \in \{\underline{\rho}_k, \overline{\rho}_k\}$
output: $\rho_{\iota,k}$

1 $\quad [x_{\iota,i,k}] = \mu_{i,k} + \left\|\rho_\iota \cdot \boldsymbol{\Gamma}_{i,k}^T\right\| \cdot [-1 \ ; \ 1] \ , \ \ i \in \{1,\ldots,n\}$
2 $\quad [\mathbf{x}_{\iota,k}] = [x_{\iota,1,k}] \times \ldots \times [x_{\iota,n,k}]$
3 $\quad [\mathbf{J}_{\mathbf{f},\iota}] = \left[\frac{\partial \mathbf{f}}{\partial \mathbf{x}_k}\right]\left([\mathbf{x}_{\iota,k}]\right)$
4 $\quad \left[\tilde{\mathbf{b}}_{\iota,k}\right] = \left(\boldsymbol{\Gamma}_{k+1}^{-1} \cdot [\mathbf{J}_{\mathbf{f},\iota}] \cdot \boldsymbol{\Gamma}_k - \mathbf{I}\right) \cdot [-1 \ ; \ 1]_{\times n}$
5 $\quad \rho_{\iota,k} = \sup\left\{\left\|\left[\tilde{\mathbf{b}}_{\iota,k}\right]\right\|\right\}$

For the computation of $\rho_{\mathrm{I},k}$ and $\rho_{\mathrm{O},k}$ in the lines 4 and 5 of Algorithm 1 according to Theorem 3, it is necessary to evaluate the Euclidean norm of the vectors $\tilde{\mathbf{b}}_{\mathrm{I},k}\left(\tilde{\mathbf{x}}_k\right)$ and $\tilde{\mathbf{b}}_{\mathrm{O},k}\left(\tilde{\mathbf{x}}_k\right)$ over the respective domains $\mathcal{E}^{\mathrm{I}}_k$ and $\mathcal{E}^{\mathrm{O}}_k$. For that purpose, both (11) and (13) are evaluated in Algorithm 2 with the help of interval analysis. For that purpose, we exploit $\tilde{\mathbf{b}}_{\mathrm{I},k}\left(\mathbf{0}\right) = \mathbf{0}$ and $\tilde{\mathbf{b}}_{\mathrm{O},k}\left(\mathbf{0}\right) = \mathbf{0}$ and perform the interval evaluation by a centered form representation.

According to Rauh and Jaulin (2021), this is given by

$$\tilde{\mathbf{b}}_{\iota,k} \in \left[\frac{\partial \tilde{\mathbf{b}}_{\iota,k}}{\partial \tilde{\mathbf{x}}_k}\right]\left([\tilde{\mathbf{x}}_k]\right) \cdot [\tilde{\mathbf{x}}_k] \ , \ \iota \in \{\mathrm{I},\mathrm{O}\} \ , \ \text{with} \tag{27}$$

$$\begin{aligned} \frac{\partial \tilde{\mathbf{b}}_{\iota,k}}{\partial \tilde{\mathbf{x}}_k}\left(\tilde{\mathbf{x}}_k\right) &= \boldsymbol{\Gamma}_k^{-1} \cdot \mathbf{A}_k^{-1} \cdot \frac{\partial \mathbf{f}}{\partial \mathbf{x}_k}\left(\mathcal{E}_k^\iota\right) \cdot \boldsymbol{\Gamma}_k - \mathbf{I} \\ &= \boldsymbol{\Gamma}_{k+1}^{-1} \cdot \frac{\partial \mathbf{f}}{\partial \mathbf{x}_k}\left(\mathcal{E}_k^\iota\right) \cdot \boldsymbol{\Gamma}_k - \mathbf{I} \quad \text{and} \end{aligned} \tag{28}$$

$$\frac{\partial \mathbf{f}}{\partial \mathbf{x}_k}\left(\mathcal{E}_k^\iota\right) \in \left[\frac{\partial \mathbf{f}}{\partial \mathbf{x}_k}\right]\left([\mathbf{x}_\iota]\right) \ , \tag{29}$$

where the interval vectors $[\mathbf{x}_\iota]$, $\iota \in \{\mathrm{I}, \mathrm{O}\}$, represent tight axis-aligned boxes enclosing the ellipsoids $\mathcal{E}_k^\iota$ for which the interval extension of the Jacobian is evaluated in (29).

These boxes, exemplarily highlighted in the upper left part of Fig. 2, are determined by finding those points $\mathbf{x}_{\iota,i}^*$ of the ellipsoids $\mathcal{E}_k^\iota$ that have an outward directed normal vector being parallel to the i-th unit vector $\mathbf{e}_i$, $\|\mathbf{e}_i\| = 1$, of $\mathbb{R}^n$. From those points, the i-th vector component is extracted to represent the box widths in the corresponding directions. Specifically, these points $\mathbf{x}_i^*$ are obtained from the collinearity condition ($\propto$ denotes proportionality)

$$\nabla\mathcal{E}_k^\iota \propto \begin{cases} \underline{\rho}_k^{-2}\boldsymbol{\Gamma}_k^{-T}\boldsymbol{\Gamma}_k^{-1}\cdot\left(\mathbf{x}_{\mathrm{I},i}^* - \boldsymbol{\mu}_k\right) = \alpha_\mathrm{I}\mathbf{e}_i & \text{for } \iota = \mathrm{I} \\ \overline{\rho}_k^{-2}\boldsymbol{\Gamma}_k^{-T}\boldsymbol{\Gamma}_k^{-1}\cdot\left(\mathbf{x}_{\mathrm{O},i}^* - \boldsymbol{\mu}_k\right) = \alpha_\mathrm{O}\mathbf{e}_i & \text{for } \iota = \mathrm{O} \end{cases} \tag{30}$$

for the normal vectors $\nabla\mathcal{E}_k^\iota$, which yields

$$\begin{aligned} \underline{\rho}_k^{-1}\boldsymbol{\Gamma}_k^{-1}\cdot\left(\mathbf{x}_{\mathrm{I},i}^* - \boldsymbol{\mu}_k\right) &= \alpha_\mathrm{I}\underline{\rho}_k\boldsymbol{\Gamma}_k^T\mathbf{e}_i \\ \overline{\rho}_k^{-1}\boldsymbol{\Gamma}_k^{-1}\cdot\left(\mathbf{x}_{\mathrm{O},i}^* - \boldsymbol{\mu}_k\right) &= \alpha_\mathrm{O}\overline{\rho}_k\boldsymbol{\Gamma}_k^T\mathbf{e}_i \ . \end{aligned} \tag{31}$$

Choosing $\alpha_\mathrm{I} = \frac{1}{\left\|\underline{\rho}_k\boldsymbol{\Gamma}_k^T\mathbf{e}_i\right\|}$ and $\alpha_\mathrm{O} = \frac{1}{\left\|\overline{\rho}_k\boldsymbol{\Gamma}_k^T\mathbf{e}_i\right\|}$ ensures that the Euclidean norm of both lines in (31) is equal to 1, and that $\mathbf{x}_{\mathrm{I},i}^*$ and $\mathbf{x}_{\mathrm{O},i}^*$ lie on the respective ellipsoid surfaces.

The line 1 of Algorithm 2 is verified by taking the i-th vector component according to $\mathbf{e}_i^T\cdot\left(\mathbf{x}_{\iota,i}^* - \boldsymbol{\mu}_k\right)$ which corresponds to

$$\left(x_{\iota,i}^* - \mu_{i,k}\right) = \begin{cases} \left\|\underline{\rho}_k\boldsymbol{\Gamma}_k^T\mathbf{e}_i\right\| & \text{for } \iota = \mathrm{I} \\ \left\|\overline{\rho}_k\boldsymbol{\Gamma}_k^T\mathbf{e}_i\right\| & \text{for } \iota = \mathrm{O} \end{cases} \tag{32}$$

and is identical to the Euclidean norms of the i-th matrix columns of $\underline{\rho}_k\boldsymbol{\Gamma}_k^T$ and $\overline{\rho}_k\boldsymbol{\Gamma}_k^T$, respectively.

Remark 6. This procedure is a generalization of the one used in Rauh and Jaulin (2021) for a one-step evaluation of nonlinear functions, where a classical, i.e., non-thick ellipsoid was assumed to be parameterized by a symmetric square-root factorization of its shape matrix. Here, the recursive evaluation typically leads to non-symmetric matrices $\boldsymbol{\Gamma}_k$ which has similarities to a lower triangular Cholesky decomposition of the thick ellipsoid's shape matrix, obtained, for example, in MATLAB by the command `chol(.,'lower')`.

4. SIMULATION RESULTS

In this section, three different scenarios for the use of the novel thick ellipsoid uncertainty representation are compared. These differ between linear and nonlinear systems, as well as models with initial conditions that are given by thick ellipsoids with either identical or different inner and outer bounds. For each of the following three scenarios, the initial ellipsoid midpoint is set to $\boldsymbol{\mu}_0 = [1\ 0.5\ 0.5]^T$.

4.1 Exactly Known Linear System Model with Thick Ellipsoid Bounds on the Initial Conditions

In analogy to Rauh et al. (2018), consider the linear system

$$\mathbf{x}_{k+1} = \mathbf{x}_k + T\cdot\left(\begin{bmatrix} 0 & 1 & 0 \\ a_{21} & a_{22} & a_{23} \\ 0 & 0 & a_{33} \end{bmatrix}\mathbf{x}_k + \begin{bmatrix} 0 \\ 0 \\ b_3 \end{bmatrix} u_k\right) \tag{33}$$

with $a_{21} = -200$, $a_{22} = -15$, $a_{23} = -400$, $a_{33} = -200$, $b_3 = 10$, the control input $u_k = 0.8\cdot x_{2,k}$, and the discretization step size $T = 10^{-3}$. The initial outer ellipsoid is a sphere with radius $R = 2^{-2}$; the inner sphere has the radius $R = 2^{-3}$ (where these values result from successively halving the radius of a unit sphere). Eq. (33) represents the temporally discretized dynamics of a spring-mass-damper system with a differentiating controller. It can be interpreted as the simplest linear representation of an active wheel suspension system with first-order lag behavior of the actuator. Fig. 3 summarizes the asymptotically stable evolution of all system states for $1,000$ time steps. To prevent ill-conditioned non-symmetric matrices $\boldsymbol{\Gamma}_k$, the shape matrix $\boldsymbol{\Gamma}_k\boldsymbol{\Gamma}_k^T$ was determined each 50-th time step and subsequently factorized by computing the symmetric matrix square root before continuing the simulation.

4.2 Uncertain Linear System Model

In the second example (step size $T = 10^{-2}$)

$$\mathbf{x}_{k+1} = \mathbf{x}_k + T\cdot\begin{bmatrix} 0 & 1 & 0 \\ -1 & -4x_{3,k}^2 & 0 \\ 0 & 0 & 0 \end{bmatrix}\mathbf{x}_k \ , \tag{34}$$

the initial state domain is characterized by a sphere of radius $R = 2^{-6}$. The dependence of the state equations on the (constant) quantity $x_{3,k}$ can be seen as an uncertain parameter-dependent model. According to Fig. 4, the outer enclosure $\mathcal{E}_k^\mathrm{O}$ starts to diverge after slightly more than 200 time steps. This results from the fact that the relation between the dynamically varying states $x_{1,k}$ and $x_{2,k}$ as well as the constant quantity $x_{3,k}$ is described by a single ellipsoid so that conservativeness in the bounds for the temporally varying states inevitably also leads to pessimism in $x_{3,k}$. In the simplest way, this can be counteracted by performing the simulation over a fixed time span (here: 100 steps), subdividing the ellipsoid afterwards equally in each space coordinate leading to a maximum of N^n (here: $N = 4$) smaller ellipsoids, running the simulation again for a fixed time span, merging all ellipsoids into one and subdividing it again before continuing the simulation.

This subdivision is based on the change of coordinates from Fig. 2 which transforms the non-axis-aligned ellipsoid into a unit sphere (coordinates $\tilde{\mathbf{x}}_k$). There, a regularly spaced rectangular mesh is intersected with the sphere, where each box is then inscribed (after backward transformation) into an ellipsoid. All ellipsoids are then propagated individually until the merging takes place. There, the same coordinate transformation is employed to a point cloud which consists of the worst-case ellipsoid widths in the coordinates $\mathbf{x}_k$ and the ellipsoid vertices in the directions of all principal axes. For those points, the maximum distance to $\tilde{\mathbf{x}}_k = \mathbf{0}$ is determined to compute a new parameter $\overline{\rho}_k$ before the next subdivision. Note, although $x_{3,k}$ was defined as a constant, its outer enclosure blows up over time. In future work, interval observers (Efimov et al., 2013) or predictor-corrector approaches (Rauh et al., 2021) will be investigated to reduce this effect.

4.3 Nonlinear System Model

As a final application, consider the extended nonlinear Brusselator model (Goubault et al., 2014; Rauh and Jaulin, 2021)

$$\mathbf{x}_{k+1} = \mathbf{x}_k + T\cdot\begin{bmatrix} 1 + x_{1,k}^2x_{2,k} - 2.5x_{1,k} + 0.5x_{3,k}^2 \\ 1.5x_{1,k} - x_{1,k}^2x_{2,k} \\ -0.5x_{3,k}^2 \end{bmatrix} \tag{35}$$

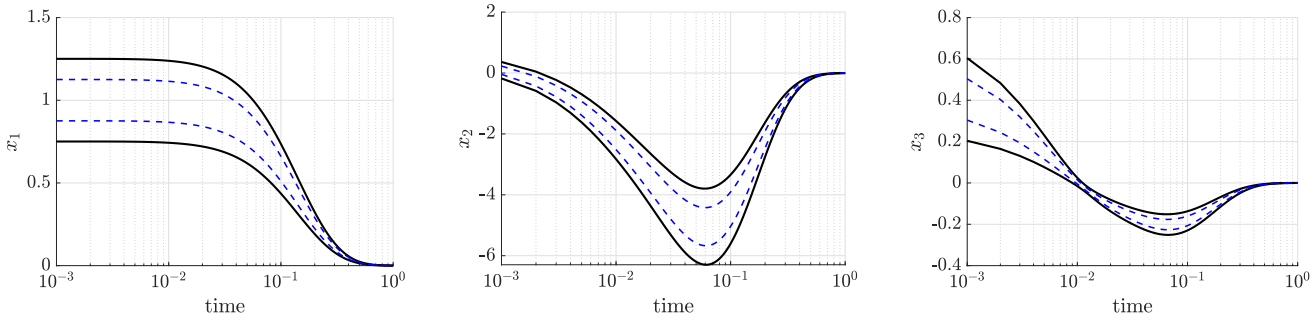

(a) State variable x_1. (b) State variable x_2. (c) State variable x_3.

Fig. 3. Simulation results for the system model (33) on a logarithmic time scale. Projections of the outer enclosures (solid lines) and inner enclosures (dashed lines).

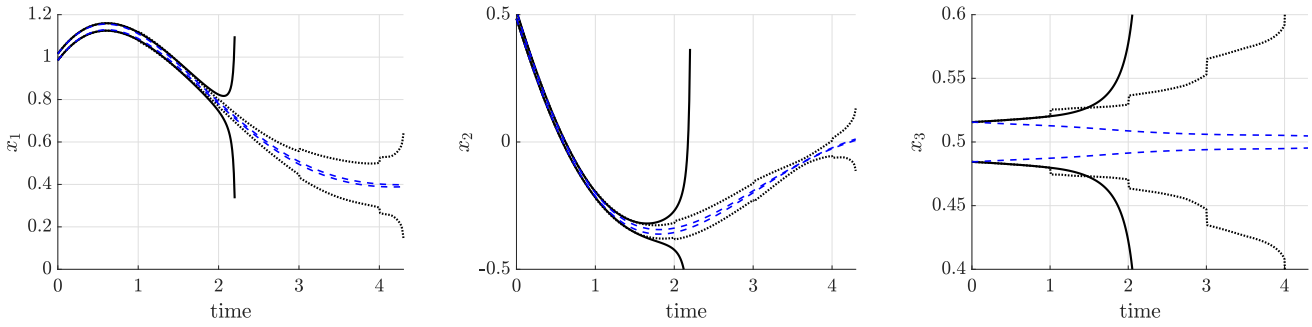

(a) State variable x_1. (b) State variable x_2. (c) State variable x_3.

Fig. 4. Simulation results for the system model (34). Projections of the outer enclosures without ellipsoid splitting (solid lines), outer enclosures with ellipsoid splitting (dotted lines) and inner enclosures (dashed lines).

with the initial sphere radius $R = 2^{-6}$. The Brusselator, discretized with $T = 0.2$, is a simple model which allows for describing oscillatory behavior in chemical reactions.

For this system, two scenarios are compared in Fig. 5. First, the simulation is performed with a single ellipsoid. In this case, the simulation breaks down with diverging outer ellipsoid bounds $\mathcal{E}_k^{\mathrm{O}}$ after 17–18 time steps. Second, to avoid this behavior, the initial domain is subdivided at $k = 0$ into smaller ellipsoids (here: $N = 8$), where no subsequent merging or further subdivisions were necessary to obtain the outer bounds (dotted lines) in Fig. 5. It can be seen that these bounds follow the dashed inner enclosure in a much tighter way than the original outer bounds. To further investigate the reason for the successful application of a single subdivision stage, Fig. 6 displays the comparison of a grid-based simulation with the outer and inner interval enclosures based on a single thick ellipsoid and additionally the outer bounds for a union of in total 408 ellipsoids ($N^3 - 408 = 104$ ellipsoids were detected to lie outside the initial domain). It can be seen that the union over all subdomains resembles a relatively thin disc, that could not be represented by a single outer enclosure.

5. CONCLUSIONS AND FUTURE WORK

In this paper, the new notion of thick ellipsoids was introduced and employed for the development of a recursive simulation routine for discrete-time dynamic systems. Based on this novel solution procedure as well as on the results of the presented fundamental strategies for domain splitting and merging, future work will deal with extending this approach towards an observer-based approach for state and parameter estimation of discrete-time systems. Moreover, observers will benefit from further investigations for efficient implementations of the union and intersection operators for thick ellipsoids mentioned in Def. 2. Finally, it is desired to employ this approach also for the simulation of continuous-time processes. Obviously, the part of a Taylor series-based solution technique that depends on the current state enclosure in tools such as VNODE-LP (Nedialkov, 2011), can be evaluated directly with the help of thick ellipsoids so that — after adding the bounds for truncation errors — a fundamental approach for finding *inner* state enclosures can be obtained.

REFERENCES

Dabbene, F. and Henrion, D. (2013). Set Approximation via Minimum-Volume Polynomial Sublevel Sets. In *Proc. of the 2013 European Control Conference (ECC)*, 1114–1119. Zurich, Switzerland.

Desrochers, B. and Jaulin, L. (2017). Thick Set Inversion. *Artificial Intelligence*, 249, 1–18.

Durieu, C., Polyak, B.T., and Walter, E. (1996). Trace Versus Determinant in Ellipsoidal Outer-Bounding, with Application to State Estimation. *IFAC Proceedings Volumes*, 29(1), 3975–3980.

Efimov, D., Raïssi, T., Chebotarev, S., and Zolghadri, A. (2013). Interval State Observer for Nonlinear Time Varying Systems. *Automatica*, 49(1), 200–205.

Goubault, E., Mullier, O., Putot, S., and Kieffer, M. (2014). Inner Approximated Reachability Analysis. In *Proceedings of the 17th Intl. Conference on Hybrid Systems: Computation and Control*, 163–172. Berlin, Germany.

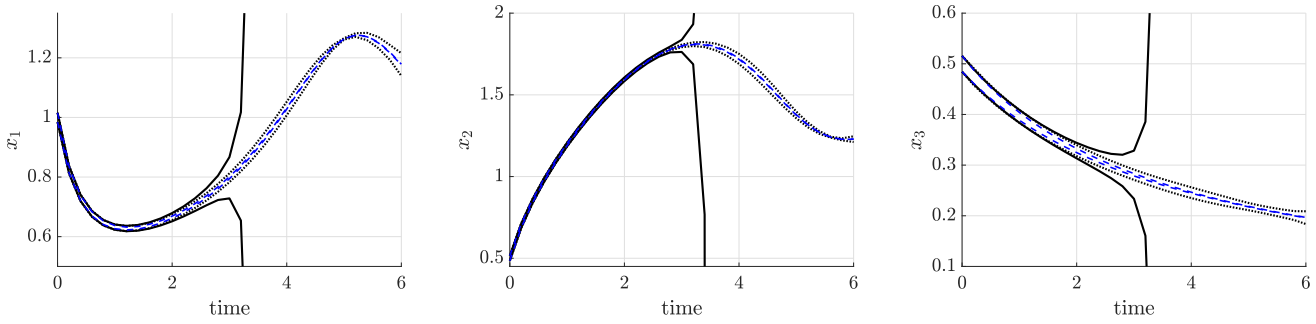

(a) State variable x_1. (b) State variable x_2. (c) State variable x_3.

Fig. 5. Simulation results for the system model (35). Projections of the outer enclosures without ellipsoid splitting (solid lines), outer enclosures with ellipsoid splitting (dotted lines), and inner enclosures (dashed lines).

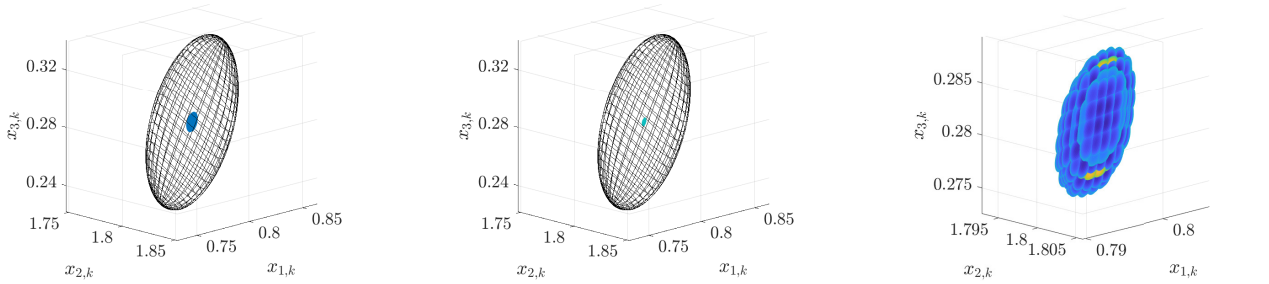

(a) Outer enclosure vs. gridding. (b) Outer enclosure vs. inner enclosure. (c) Outer enclosure (with splitting).

Fig. 6. State enclosures at the time step $k = 15$ (time $t = 3.0$); Figs. 6(a) and 6(b) without splitting.

Jaulin, L., Kieffer, M., Didrit, O., and Walter, É. (2001). *Applied Interval Analysis*. Springer–Verlag, London.

Kurzhanskii, A.B. and Vályi, I. (1997). *Ellipsoidal Calculus for Estimation and Control*. Birkhäuser, Boston, MA.

Kurzhanskiy, A. and Varaiya, P. (2006). Ellipsoidal Toolbox (ET). In *Proceedings of the 2006 IEEE Conference on Decision and Control*, 1498–1503. San Diego, CA, USA.

Mazenc, F. and Bernard, O. (2010). Asymptotically Stable Interval Observers for Planar Systems With Complex Poles. *IEEE Transactions on Automatic Control*, 55(2), 523–527.

Moore, R., Kearfott, R., and Cloud, M. (2009). *Introduction to Interval Analysis*. SIAM, Philadelphia.

Nedialkov, N. (2011). Implementing a Rigorous ODE Solver through Literate Programming. In A. Rauh and E. Auer (eds.), *Modeling, Design, and Simulation of Systems with Uncertainties*, Mathematical Engineering. Springer–Verlag, Berlin, Heidelberg.

Neumaier, A. (1993). The Wrapping Effect, Ellipsoid Arithmetic, Stability and Confidence Regions. In R. Albrecht, G. Alefeld, and H.J. Stetter (eds.), *Validation Numerics: Theory and Applications*, 175–190. Springer–Verlag, Vienna.

Rauh, A. and Kersten, J. (2020). From Verified Parameter Identification to the Design of Interval Observers and Cooperativity-Preserving Controllers. *Acta Cybernetica*, 24(3), 509–537.

Rauh, A., Kersten, J., and Aschemann, H. (2019). Techniques for Verified Reachability Analysis of Quasi-Linear Continuous-Time Systems. In *Proc. of 24th Intl. Conf. on Methods and Models in Automation and Robotics 2019*. Miedzyzdroje, Poland.

Rauh, A., Kletting, M., Aschemann, H., and Hofer, E.P. (2007). Reduction of Overestimation in Interval Arithmetic Simulation of Biological Wastewater Treatment Processes. *Journal of Computational and Applied Mathematics*, 199(2), 207–212.

Rauh, A., Romig, S., and Aschemann, H. (2018). When is Naive Low-Pass Filtering of Noisy Measurements Counter-Productive for the Dynamics of Controlled Systems? In *Proc. of 23rd Intl. Conf. on Methods and Models in Automation and Robotics MMAR 2018*. Miedzyzdroje, Poland.

Rauh, A., Bourgois, A., and Jaulin, L. (2021). Union and Intersection Operators for Thick Ellipsoid State Enclosures: Application to Bounded-Error Discrete-Time State Observer Design. *Algorithms*, 14(3). URL `https://www.mdpi.com/1999-4893/14/3/88`.

Rauh, A. and Jaulin, L. (2021). A Computationally Inexpensive Algorithm for Determining Outer and Inner Enclosures of Nonlinear Mappings of Ellipsoidal Domains. *Applied Mathematics and Computer Science AMCS*. Under review.

Stolfi, J., Figueiredo, L., and Dona, E. (2003). An Introduction to Affine Arithmetic. *TEMA. Tendências em Matemática Aplicada e Computacional*, 4.